Testing extreme warming and geographical heterogeneity

María Dolores Gadea Rivas [*] University of Zaragoza

Jesús Gonzalo [†] U. Carlos III de Madrid

Jose Olmo [‡] U. of Zaragoza and U. of Southampton

February 15, 2024

Abstract

Understanding the heterogeneity in worldwide temperatures is important for predicting future dynamics in climate change and guide policy. In this paper, we propose analytical methods to analyze the dynamics of extreme temperatures and, in particular, to detect the presence of time trends in the tail parameters driving the tail decay of the distribution of annual temperatures. As a byproduct, we study the performance of Hill type estimators of the tail parameter under the presence of different location effects and propose a version of the estimator obtained from the standardized order statistics that performs better in finite samples. Our empirical results for the analysis of eight regions covering the Globe over the period 1960 to 2022 show clear heterogeneity in the warming process of extreme temperatures. We find four patterns in the warming process of extreme temperatures. The extreme positive temperatures of North America, Asia and the Antarctic region are trending up faster than for the remaining regions. Europe, Africa and the Arctic region do not exhibit warming in the extremes despite a steady increase in their quantiles suggesting that the warming process takes place in the low and high quantiles and not in the extremes. South America and Australia show warming of extreme temperatures in the left tail but no warming on the right tail. In fact, for these regions the dispersion in the distribution of temperatures is falling over time. All these findings provide some evidence of geographical clustering in the evolution of extreme temperatures over time.

JEL classification: C31, C32, Q54

[*] Department of Applied Economics, University of Zaragoza. Gran Vía, 4, 50005 Zaragoza (Spain). Tel: +34 9767 61842, and e-mail: lgadea@unizar.es

[†] Department of Economics, University Carlos III, Madrid 126 28903 Getafe (Spain). Tel: +34 91 6249853, and e-mail: jesus.gonzalo@uc3m.es

[‡] Department of Economic Analysis, University of Zaragoza. Gran Vía, 4, 50005 Zaragoza (Spain). Tel: +34 876 55 4682, and e-mail: joseolmo@unizar.es (corresponding author)

1 Introduction

Growing empirical evidence of a gradual warming trend in global mean temperature (Hansen and Lebedeff, 1987, 1988) has led to a heightened awareness of human-induced climate change through pollution and carbon emissions. This evidence is not only observed for mean temperatures but across different distributional characteristics (see Gadea and Gonzalo (2020, 2024), GG2020 and GG2024 hereafter) indicating that warming is a global phenomenon. These authors also find that the occurrence of global warming is heterogeneous and takes place at different speeds across quantiles and regions. In particular, GG2020 find an increasing trend in all distributional characteristics (time series and cross-sectional) when analyzing temperatures from all available weather stations in the Globe. The trend is for most regions larger in the lower quantiles than in the mean, median, and upper quantiles. Relatedly, there is a negative trend in the characteristics that measure dispersion such as the standard deviation and the interquartile range (i.e., lower temperatures approach the median faster than higher temperatures do). GG2024 extend this study by considering different regions separately. These authors also introduce the idea of geographic heterogeneity in the warming process and define four different types of warming based on the type of trend the quantile process exhibits. These authors do not study, though, the presence of trends in the dynamics of extreme temperatures below the 5% quantile and beyond the 95% quantile. Therefore, the conclusions of this study cannot fully reveal the presence of warming in the extreme temperatures and whether the dynamics of these observations show geographical heterogeneity that can reveal important insights about what sort of extreme events different regions can expect as a result of a warming planet. The aim of the current study is to address these questions.

Extreme events act as a catalyst for concern about whether the climate is changing. Assessments of the economic impacts of global climate change have usually focused on averages, rather than on variability or extremes (Adams et al, 1990), but the primary impacts of climate on society result from extreme events, a reflection of the fact that climate is inherently variable. In spite of the need to examine how the frequency of extreme events might change as the mean climate changes (Wigley, 1985; Mitchell et aL, 1990), attempts to quantify the nature of such relationships have been rare (Mearns et al, 1984; Wigley, 1988). Katz and Brown (1992) is one of the first examples to study the relative sensitivity of extreme events to the mean and variability (more generally, the location and scale parameters) of climate. In their pioneering study, these authors find that extreme events are relatively more sensitive to the variability of climate than to its average and

this sensitivity is relatively greater the more extreme the event. To do this, these authors consider a model in which climate change is envisioned to involve a combination of two different statistical operations given by a change in location or a change in scale parameter. GG not only consider changes in these parameters but also the presence of time trends strengthening the impact and severity of climate change.

Following the work of Katz and Brown (1992) and GG2020, we aim to extend their analyses of distributional characteristics by focusing on the dynamics of extremes. We focus on the tail parameter that fully characterizes the behavior of the distribution in the tails, see Embrechts, Kluppelberg and Mikosch (1997). Our aim is to understand if the increased likelihood of extreme events recently observed in climate variables is due to the positive trends in distributional characteristics such as the mean and the quantile process, as observed in GG2020 and GG2024, or to the increase of extreme termperatures. We aim to capture these increases in the form of time trends in the tail parameter estimates. To do this, we adapt the tests developed in GG2020 and GG2024 to assess statistically the presence of trends and cotrends of unknown form in the tail parameter. In order to apply these tests, we replace the distributional characteristics with the empirical counterparts given by consistent estimates of the shape parameter. This parameter is specific to each tail and fully characterizes the pattern of tail decay and, therefore, the fatness of the tail. We focus on the Hill (1975) estimator and the efficient regression-based estimator developed in Gabaix and Ibragimov (2012) of the tail parameter (see also Rosen and Resnick (1980); Gabaix (1999); Gabaix and Ioannides (2004), among others).

Our second contribution is to study the finite-sample effects of estimating the tail parameter directly from location-scale transformations of the distribution generating the tail events and not from standardized versions of the data. This is a necessary step to be able to identify the source of dynamics in extreme events. These dynamics can be due to location-scale shifts of the parent distribution of observations over time, to increases in the likelihood of extreme events (heavier tails) once location-scale effects are controlled for or to both. To do this, we study the performance of Hill and regression-based estimators of the tail parameter in location-scale families of distributions. We derive analytically the presence of a wedge in the Hill estimator obtained from raw and standardized versions of the order statistics. This effect vanishes asymptotically as both versions of the Hill estimator provide consistent estimates of the tail parameter as the sample size increases, however, we analytically derive potentially sizeable differences between versions of the estimators due to location effects. These insights are illustrated in a simulation study with

data obtained from Student-t distributions with different degrees of freedom. The empirical results provide evidence of finite-sample differences in the estimation of the tail parameter even for very large sample sizes. The estimators of the tail parameter obtained from standardized order statistics outperform the estimators obtained from the raw sequences if the location parameter is large in magnitude. For small values of the location parameter the estimates obtained from the unstandardized estimators are comparable and even superior to the standardized ones. However, the results are not uniform across tail behaviors, thus, we find overwhelming support for the standardized versions of the Hill estimator for heavy tailed distributions whereas the unstandardized estimators perform better as the tail decay approaches the exponential case.

These methods are applied in an empirical application to eight regions (the Antarctic region, the Arctic, Africa, Asia, Australia, Europe, North America and South America) covering the Globe over the period 1960 to 2022. Using a panel of observations on monthly temperatures from a large cross section of weather stations, we estimate the tail parameters from cross-sectional distributions applied to each of these regions and obtain time series of tail parameter estimates for each tail of the distribution. Our empirical results show clear heterogeneity in the warming process of extreme temperatures across regions. There are, however, four clear patterns that seem related to the geographical location of the regions under investigation. Thus, North America, Asia and the Antarctic region are affected by a warming process that we denominate of type WE2 and corresponds to warming in the extreme positive temperatures whereas the extreme temperatures in the left tail do not show evidence of warming. In contrast, the Polar region, Europe and Africa do not exhibit warming in the extremes despite the steady increase in their quantiles found in GG2020. In the Southern hemisphere, the warming process of extreme temperatures for South America and Australia is observed in the left tail and is characterized by milder minimum temperatures compared to previous years. The evidence obtained from the tail parameter estimates for this tail suggests that extreme negative quantiles trend faster to the right of the distribution than the process of low quantiles. We denominate the type of warming observed in the left tail as WE1. In contrast, for these regions, the dynamics of positive extreme temperatures show evidence of the opposite, that is, the trend of the tail parameter is negative indicating a stronger trend for high quantiles than for extreme quantiles. This phenomenon can be interpreted as evidence of no extreme warming in the right tail.

The paper is structured as follows. Section 2 reviews basic results on EVT and tail

behavior under Pareto type approximations. Section 3 applies the results on EVT to time series and introduces several definitions of warming in the extremes. The section also discusses several tests to detect the presence of trends of general form in distributional characteristics. In our framework, we focus on modeling the dynamics of the tail parameter. Section 4 reviews popular estimators of the tail parameter such as the Hill estimator and regression-based estimators, and derives analytically and numerically the presence of finite-sample discrepancies between versions of these estimators constructed from unstandardized and standardized sequences of order statistics. Section 5 presents an empirical application to a panel of monthly temperatures for analyzing the dynamics of the tail parameter in both tails of the distributions. We divide the Globe into eight regions and construct time series estimates of the tail parameters obtained from cross-sectional data on temperatures recorded from weather stations. We analyze the warming patterns of extreme temperatures in both tails and classify the regions according to their warming type. Section 6 concludes. Tables and figures are found at the end of the document.

2 Background theory

This section introduces some background theory required to understand the models and methods introduced below.

2.1 Basic results on extreme value theory

Extreme Value Theory (EVT) studies the limiting distribution of the standardized maxima (and minima) of a random sample $\{X_i\}_{i=1}^n$ of size n. Let $M_n = \max\{X_1, \ldots, X_n\}$ be the sample maximum and let $F(x)$ denote the probability law generating such observations. Gnedenko (1943) and de Haan (1976) characterize the lim.iting distribution of the standardized maximum. More formally, there are normalizing sequences a_n and b_n such that $P\{a_n^{-1}(M_n - b_n) \leq x\} \to G(x)$, as $n \to \infty$, with $G(x) = e^{-\tau(x)}$. This result is further refined depending on the maximum domain of attraction of the parent distribution $F(x)$. Thus, $\tau(x)$ can only be of three forms: (i) Type I (Gumbel): $\tau(x) = e^{-x}$ for $x \in (-\infty, \infty)$; (ii) Type II (Fréchet): $\tau(x) = x^{\xi}$ for $x > 0$ and $\xi > 0$; (iii) Type III (Weibull): $\tau(x) = -(-x)^{-\xi}$ for $x < 0$ and $\xi < 0$. The three types of extreme value distributions can be expressed in the so-called Generalized Extreme Value Distribution, first proposed by von Mises (1936), and given by $G(x) = e^{-\tau(x)}$ with $\tau(x) = \left(1 + \frac{1}{\xi}x\right)^{-\xi}$ for $\xi \neq 0$, and $\tau(x) = e^{-x}$, for $\xi = 0$. The distribution of the standardized maximum is fully characterized by the shape parameter ξ.

This parameter is the inverse of the so-called tail index used in the EVT literature. For notational convenience, we will hereafter use tail parameter to refer to the shape parameter ξ introduced above and ttail index ψ to refer to its inverse.

The above asymptotic results for the distribution of the maximum for independent and identically distributed (iid) data also implies the following approximation $n(1 - F(a_n x + b_n)) \to \tau(x)$,for a_n and b_n suitable sequences and x sufficiently large. The function $\tau(x)$ and, in particular, the tail parameter ξ determine the behavior of the distribution in the right tail. Broadly speaking, a positive value of the tail parameter indicates a polynomial decay of the distribution in the tail and, hence, the presence of heavy tails. More formally, a heavy-tailed distribution is defined as a distribution function $F(x)$ such that

$$1 - F(x) = x^{-\xi}\mathcal{L}(x), \tag{1}$$

where $\mathcal{L}(x)$ is a slowly varying functon satisfying $\lim_{t\to\infty} \frac{\mathcal{L}(tx)}{\mathcal{L}(t)} = 1$ for $x > 0$. Values of ξ in the interval $(0, 20)$ are usually identified with the presence of heavy tails and the scenario $\xi > 20$ corresponds to a tail with exponential decay. The case $\xi \leq 2$ corresponds to very heavy tailed distribution functions characterized by infinite variance, and $\xi \leq 1$ by a distribution function with no mean. Interestingly, for the Student-t family of distributions, the tail parameter coincides with the degrees of freedom coefficient.

Remark 1: The above asymptotic results show that location-scale transformations of the parent distribution $F(x)$ do not affect its tail behavior. Location and scale parameters are incorporated in the asymptotic results through suitable transformations of the sequences a_n and b_n.

Remark 2: Let $Y = \mu+\sigma X$ denote a location (μ) - scale (σ) transformation of the standard random variable X. Let F_x be the distribution function of X that satisfies condition (1). It follows that

$$1 - F_y(y) = 1 - F_x\left(\frac{y-\mu}{\sigma}\right) = \left(\frac{y-\mu}{\sigma}\right)^{-\xi} \mathcal{L}\left(\frac{y-\mu}{\sigma}\right), \tag{2}$$

for $y > \mu + \sigma$. The tail of the parent distribution $F(y)$ can be approximated by the tail of a Pareto distribution for y sufficiently large.

Remark 2 shows that the probability of extreme events in location-scale models is completely characterized by the location and scale parameters μ and σ, respectively, and the tail parameter ξ. To show this, let $x > 0$ denote an extreme positive event associated

to the random variable X. Following expression (1), the probability of the extreme event is $P\{X > x\} \approx x^{-\xi^R}$, with ξ^R the tail parameter driving the behavior in the right tail. Under a location-scale transformation of the random variable, the probability of the same extreme event is $P\{Y > x\} \approx \left(\frac{x-\mu}{\sigma}\right)^{-\xi^R}$. The probability increases with the location and scale parameters and decreases with the tail parameter ξ. In contrast, the probability of an extreme event of same magnitude $-x$ in the left tail is $P\{X \leq -x\} \approx x^{-\xi^L}$ where ξ^L denotes the tail parameter driving the behavior in the left tail. Similarly, for the location-scale transformation, it follows that $P\{Y \leq -x\} \approx \left(\frac{x+\mu}{\sigma}\right)^{-\xi^R}$. In contrast to the right tail, for the left tail, the probability of extreme events decreases as the location parameter rises. The relationship between the other two parameters (scale and tail behavior) and the probability of positive extremes is the same as for the right tail.

3 Modeling dynamics in extreme temperatures

The above results modeling the probability of extreme events can be adapted to modeling the dynamics of extreme temperatures over time. In GG2020 temperature is viewed as a functional stochastic process $X = (X_t(\omega), t \in T)$, where T is an interval in $\mathbb{R}$ defined in a probability space $(\Omega, \Im, P)$. A convenient example of an infinite-dimensional discrete-time process consists of associating $\nu = (\nu_n, n \in \mathbb{R}^+)$ with a sequence of random variables whose values are in an appropriate function space. This may be obtained by setting

$$X_t(n) = \nu_{t,N+n},\ 0 \leq n \leq N,\ t = 0, 1, 2, \ldots, T$$

so $X = (X_t, t = 0, 1, 2, \ldots, T)$. If the sample paths of ν are continuous, then we have a sequence $X_0, X_1, \ldots$ of random variables in the space $C[0, N]$. In this case t will be the period of a year, and N represents cross-sectional units (climate stations recording data).

In contrast to GG2020 and GG2024 that focus on modeling a battery of distributional characteristics such as the mean, median and quantile process, our interest in this paper is in modeling the tail behavior of the sequence of distribution functions $(F_{y1}, \ldots, F_{yT})$. This is given by the sequence of tail parameters $(\xi_1(\omega), \ldots, \xi_T(\omega))$. These distributional characteristics can be considered time series objects and, therefore, all the econometric tools already developed in the time series literature can be applied to $\xi_t(\omega)$.

Following the above results, the probability of extreme temperatures in the left tail at time t is modeled as

$$P\{X_t \leq -x\} = C^L \left(\frac{x + \mu_t}{\sigma_t}\right)^{-\xi_t^L} \tag{3}$$

where μ_t and σ_t denote the time-varying location and scale parameters, respectively, ξ_t^L denotes the tail parameter characterizing the behavior in the left tail and C^L is a suitable constant. Similarly, the probability of extreme temperatures in the right tail at time t is modeled as

$$P\{X_t > x\} = C^R \left(\frac{x - \mu_t}{\sigma_t} \right)^{-\xi_t^R} \tag{4}$$

with ξ_t^R denoting the tail parameter characterizing the behavior in the right tail and C^R a suitable constant.

GG2020 define warming as an increasing trend in certain characteristics of the temperature distribution. More precisely, warming is defined as the existence of an increasing trend in some of the characteristics measuring the central tendency or position (quantiles) of the temperature distribution. GG2024 introduce three characterizations of the warming process depending on the relative speed across quantiles $q_t(\tau)$, with $\tau \in (0, 1)$, of the location parameters associated to each τ driving their dynamics. More formally,

Definition 1 (Typology of warming process):

- **W0**: There is no trend in any of the quantiles (No warming).
- **W1**: All the location distributional characteristics have the same positive trend (dispersion does not contain a trend).
- **W2**: The Lower quantiles have a larger positive trend than the Upper quantiles (dispersion has a negative trend).
- **W3**: The Upper quantiles have a larger positive trend than the Lower quantiles (dispersion has a positive trend).

Following these characterizations of the warming process, we introduce further characterizations based on the behavior of the process of temperatures in the extremes. Note that the approach used by GG2020 and GG2024 is silent about the dynamics of extreme events as their methods are not devised to capture the behavior of temperatures in the extremes. In this paper, we capture these dynamics through the evolution of the tail parameter over time. This is formalized in the following definition.

Definition 2 (Warming Extremes): We define three possible warming scenarios characterized by extreme temperatures:

- **WE0**: There is no trend in any of the tail parameters ξ_t^L and ξ_t^R.
- **WE1**: The tail parameter ξ_t^L has a positive trend.
- **WE2**: The tail parameter ξ_t^R has a negative trend.

WE0 describes a scenario with no warming in the extreme temperatures. The likelihood of extreme events remains constant over time and is characterized by the tail parameter ξ^L; WE1 characterizes a scenario given by warming in the extreme temperatures in the left tail. An increase in the tail parameter over time implies a decrease in the fatness of the tail and, therefore, a smaller probability of the tail event. This relationship can be observed from expression (3) for fixed values of μ and σ. Similarly, WE2 characterizes a scenario given by an increase in the extreme positive temperatures over time. These scenarios can be related to the types of warming defined in GG2024.

Proposition 1: Let $W0-W3$ be the warming scenarios introduced in Definition 1. Then, $W1 \Rightarrow WE0$; $W2 \Rightarrow WE1$; $W3 \Rightarrow WE2$.

The proof of these results is as follows. $W1 \Rightarrow WE0$ follows from observing that W1 implies the same location effect affecting all quantiles of the distribution of temperatures. Remark 1 shows that this type of effects does not have an impact on the tail decay of the parent distribution. To prove $W2 \Rightarrow WE1$, we note that scenario W2, taken at face value, entails a warming process in which the extreme quantiles in the left tail of the distribution ($q_t(\tau)$, for $\tau \approx 0$) trend up faster than the low quantiles characterized by $\tau^{'} > \tau$. This implies a reduced dispersion in the left tail of the distribution and, hence, an increase of the tail parameter ξ_t^L over time (decrease in the tail index). WE1 implies a warming process for the extreme temperatures characterized by minimum temperatures rising faster than the rest. Finally, to show the condition $W3 \Rightarrow WE2$, we note that Scenario W3, taken at face value, implies the opposite. The high quantiles ($q_t(\tau)$) drift apart from the extreme quantiles ($q_t(\tau^{'})$, for $\tau^{'} \approx 1$ and $\tau < \tau^{'}$) in the right tail such that the tail parameter ξ_t^R decreases over time (tail index increases). In this type of warming extreme positive temperatures become more frequent and the likelihood of even more extreme temperatures also increases over time.

Interestingly, the warming scenarios $W0 - W3$ are mutually exclusive, however, our characterization of the warming process in the extremes allows for WE1 and WE2 to take place simultaneously as these phenomena refer to different tails. We can observe two types

of warming in the extremes for the same region. A particularly concerning scenario is given by WE1 and WE2 together. Importantly, the empirical application of the methods in GG2020 and GG2024, and Definition 1 above, do not span below the quantiles $\tau = 0.05$ and beyond $\tau = 0.95$. Therefore, the methodology proposed in these papers is not able to capture the presence of trends in extreme events. In this paper, we address this shortcoming by modeling the presence of trends in the extremes through the tail parameters ξ_t^L and ξ_t^R. To do this, we adapt the definition of Warming in GG2024.

Definition 3: The tail parameter ξ_t obtained from the sequence of distribution functions $F_t(\cdot)$ contains a trend if in the LS regression,

$$\xi_t = \alpha + \beta t + u_t,\ t = 1, \dots T, \tag{5}$$

the hypothesis $H_0 : \beta = 0$ is rejected. This hypothesis can be tailored to specify if the trend is positive or negative.

Importantly, GG2020 shows that a simple t-test for the hypothesis $\beta = 0$ is able to detect most of the existing deterministic trends (polynomial, logarithmic, exponential, etc) and also the trends generated by any of the three standard persistent processes considered in the literature: (i) fractional or long-memory models ($1/2 < d < 3/2$); (ii) near-unit-root AR models; and (iii) local-level models. Furthermore, if the regression (5) is the true data-generating process, with u_t a stationary process, then the distribution of the t-test under the null hypothesis is $N(0, 1)$. GG2020 recommend to use a robust HAC version of the t-test.

Using a similar methodology, we adapt the above definition to detect the presence of cotrending in tail behavior across different regions.

Definition 4: The tail parameters ξ_t^x and ξ_t^y obtained from the sequence of distribution functions $F_t^x(\cdot)$ and $F_t^y(\cdot)$ are cotrended if in the LS regression,

$$\xi_t^x - \xi_t^y = \alpha + \gamma t + u_t,\ t = 1, \dots T, \tag{6}$$

the hypothesis $H_0 : \gamma = 0$ is rejected.

This method can be adapted to test symmetry in tail behavior over time for a single sequence of distribution functions. Empirically, this is not relevant for the purpose of this study since extreme warming in each tail is characterized by tail parameters of different sign.

4 Estimation of the tail parameters

The above methods are unfeasible in practice since the sequence of tail parameters is not observed. Following GG2020, we propose to estimate these parameters using cross-sectional information from climate stations around the Globe. We assume the data on temperatures to be *iid* and is used to estimate the tail parameters ξ_t^L and ξ_t^R from a sample of N observations. By doing so, we construct a time series of estimates $(\widehat{\xi}_1, \ldots, \widehat{\xi}_T)$ that is used for testing for the presence of trends in both tails.

4.1 Review of popular estimators

Estimation of the tail parameter is cumbersome as it depends, for most estimators, on a nuisance parameter that establishes the number of observations defining the tail of the distribution. Despite this difficulty or perhaps because of it, the EVT literature has developed more than one hundred estimators, see Fedotenkov (2018). Early and popular estimators such as the Hill (1975) and Pickands (1975) estimators are derived as conditional maximum likelihood estimators of Pareto and Generalized Pareto distributions, respectively, fitting the tails of a broad class of parent distributions. The version of the Hill estimator for the shape parameter ξ^R introduced above is

$$\widehat{\xi}_H^R = \left[\frac{1}{k} \sum_{i=1}^{k} log\left(x_{i:n} / x_{k+1:n} \right) \right]^{-1}, \tag{7}$$

where $x_{1:n} > \ldots > x_{k+1:n}$ denote the first $k+1$ order statistics of the random sample $(x_1, \ldots, x_n)$. The order statistic $x_{k+1:n}$ can be interpreted as the threshold value that determines the Pareto behavior in the tail of the parent distribution. Hill's estimator is consistent for $\xi > 0$ under suitable choices of $x_{k+1:n}$ as long as the latter sequence is characterized by the intermediate sequence $k \to \infty$ with $k/n \to 0$ as $n \to \infty$. Pickands' (1975) estimator of the tail parameter ξ^R is defined as

$$\widehat{\xi}_P^R(i) = \frac{log(2)}{log\left((x_{i:n} - x_{2i:n}) / (x_{2i:n} - x_{4i:n}) \right)}, \quad \text{for } i = 1, \ldots, k. \tag{8}$$

In constrat to Hill estimator, Pickands' estimator is consistent for any $\xi \in \mathbb{R}$ and intermediate sequence $k \to \infty$ with $k/n \to 0$. Another important advantage of the latter estimator is its invariance under shift and scale transformations of the observations. A refined version of the estimator (8) is provided by Drees (1995). This author introduces an estimator of ξ^R

that is constructed as a weighted mixture of Pickands' estimators computed over different values of $i = 1, \ldots, k$. The weights are generated by a probability measure which satisfies certain integrability condition. Unfortunately, the finite-sample performance of Pickand's type estimators is not very satisfactory in small and moderate sample sizes.

Other well known consistent estimators of the tail index based on the above estimators are the moment estimator of Dekkers, Einmahl and de Haan (1989), the method of moments ratio estimator proposed in Danielsson, Jansen and De Vries (1996), and more recently, the generalized least square estimator of Aban and Meerschaert (2004) and the least squares estimator of Tripathi (2014). A shortcoming common across these methods is their questionable performance in small samples. Huisman et al (2001) correct for the small-sample biases in these methods by constructing a weighted average of a sequence of tail index estimators obtained from different thresholds $x_{k+1:n}$.

An alternative approach to estimate the tail parameter is to plot the statistic of interest against a number of the sample upper-order statistics and then infer an appropriate value for the tail index from the properties of the resulting graph (Kratz and Resnick, 1996; Beirlant et al., 1996). Inspired by this approach, regression-based estimation methods have attracted considerable attention among empirical researchers. One such alternative is the OLS-based log-log rank-size regression (Rosen and Resnick, 1980 and Gabaix, 1999) that is given by the OLS estimator from the regression

$$log(i - \gamma) = \alpha_0 - \xi^R log x_{i:n} + \varepsilon_i, \text{ with } i = 1, \ldots, k, \tag{9}$$

with $\gamma = 0$ and ε_i an error term. The statistical properties of the OLS estimators of equation (9) have been analyzed in Gabaix and Ioannides (2004) and Gabaix and Ibragimov (2012). The latter authors also propose an optimal version of this type of estimators given by considering $\gamma = 1/2$. A shortcoming of most of these methods is their sensitivity to location transformations of the data. This is studied in more detail below. A notable exception is the recent regression-based estimator of Nicolau and Rodrigues (2019). These authors provide an important improvement over the above estimators by reducing the bias, being resilient to the choice of the tail length and accommodating time dependence in the data. Nevertheless, we focus on the most popular estimators so far given by Hill type estimators and regression-based estimators of the tail parameter.

4.2 Finite-sample effects on tail parameter estimates

The above battery of estimators of the tail parameter are statistically consistent, implying their convergence in probability to the true parameter as the sample size increases. There are, however, relevant finite-sample effects[1] that hold even in very large samples due to the slow convergence rate ($\sqrt{k}$) of most estimators that may conflict with large values of the location parameters under the presence of time trends. These trends appear as time fixed effects in the panel structure of our data. As mentioned above, estimation is done using cross-sectional information only and assuming that the distribution function of cross-sectional temperatures varies over time.

In what follows, we explore the role of the location and scale parameter in more detail and derive the finite-sample differences between the versions of the Hill estimator obtained from standardized and unstandardized data. Let $Y = \mu + \sigma X$ denote a random variable with mean μ and variance σ, and let X be the standardized counterpart. Similarly, let $y_{1:n} > \ldots > y_{k+1:n}$ and $x_{1:n} > \ldots > x_{k+1:n}$ denote the sequence of order statistics of Y and X, respectively, with $x_{i:n} = (y_{i:n} - \mu)/\sigma$, for $i = 1, \ldots, n$. For analytical convenience, we operate with the inverse of the tail parameter ξ^R that is denominated in the EVT literature as tail index and denoted hereafter as $\psi^R \equiv 1/\xi^R$.

The Hill estimator applied to the tail index ψ^R and obtained from an *iid* realization of the random variable Y is given by $\widehat{\psi}_H^R = \frac{1}{k}\sum_{i=1}^{k} log\left(x_{i:n}/x_{k+1:n}\right)$ whereas the estimator constructed from the standardized version of the order statistics, denoted as $\widehat{\psi}_H^{sR}$ is defined similarly and satisfies that

$$\widehat{\psi}_{Hs}^R = \frac{1}{k}\sum_{i=1}^{k} \log \frac{y_{i:n} - \widehat{\mu}}{\widehat{\sigma}} - log\frac{y_{k+1:n} - \widehat{\mu}}{\widehat{\sigma}} = \widehat{\psi}_H^R + \frac{1}{k}\sum_{i=1}^{k} \log\left(1 - \frac{\widehat{\mu}}{y_{i:n}}\right) - \log\left(1 - \frac{\widehat{\mu}}{y_{k+1:n}}\right), \tag{10}$$

with $\widehat{\mu}$ and $\widehat{\sigma}$ denoting consistent estimators of the location and scale parameters μ and σ, respectively. Simple algebra shows that the estimator $\widehat{\psi}_{Hs}^R$ can be decomposed as

$$\widehat{\psi}_{Hs}^R = \widehat{\psi}_H^R + \widehat{\psi}_u^R + \widehat{\psi}_r^R, \tag{11}$$

with $\widehat{\psi}_u^R = \frac{1}{k}\sum_{i=1}^{k} log\frac{u_{i:n}}{u_{k+1:n}}$, where $u_{i:n} = 1 - \mu/y_{i:n}$, for $i = 1, \ldots, k+1$. There is an additional

[1] See Aban and Meerschaertt (2001) that propose a shifted Hill estimator that is more robust for estimating the tail decay of heavy-tailed distributions.

term in the decomposition given by $\widehat{\psi}_r^R = \frac{1}{k}\sum_{i=1}^{k} log\frac{r_{i:n}}{r_{k+1:n}}$, with $r_{i:n} = 1 - (\widehat{\mu} - \mu)/(x_{i:n} - \mu)$, that captures the estimation of the location and scale parameters in the tail index estimator. The latter term, as formalized below, converges to zero in probability if the estimator of the location parameter $\widehat{\mu}$ converges to μ at a rate higher than $\sqrt{k}$. Standard parametric estimators such as the sample mean satisfy this condition. Importantly, the Hill estimator is invariant to the scale parameter implying that estimates of the tail behavior of a distribution do not depend on scale transformations of the data.

It is of more interest to explore the asymptotic behavior of $\widehat{\psi}_u^R$. For μ fixed, this is driven by the limiting convergence of the extreme order statistics $y_{i:n}$, with $i = 1, \ldots, k+1$, where $k \to \infty$ and $k/n \to 0$. This condition entails the divergence of the order statistics to infinity (for unbounded distributions) such that $\widehat{\psi}_u^R \xrightarrow{p} 0$, as the sample size increases, and follows that $\widehat{\psi}_{Hs}^R - \widehat{\psi}_H^R \xrightarrow{p} 0$. Using simple algebra, this result also implies the convergence in probability between the estimators of the tail parameter ξ^R such that $\widehat{\xi}_{Hs}^R - \widehat{\xi}_H^R$ as $n \to \infty$.

This result is, however, quite misleading in finite samples since the magnitude of the location parameter μ and the speed of divergence of the order statistics (driven by the tail behavior of the distribution) have an important effect on the estimates of the Hill estimator in finite samples. The following section illustrates these effects in finite samples and extends the analysis to regression-based estimators.

4.3 Simulation exercise

The following simulation experiment compares the finite-sample performance of the Hill estimator in (7) and Gabaix and Ibragimov's (2012) regression-based estimator introduced in (9). The aim of the simulation exercise is to assess the empirical performance of these estimators and compare it against the performance of the estimators constructed from standardized order statistics. We consider four estimators of the tail parameter ξ^R shaping the decay of the parent distribution on the right tail: (1) Hill estimator in (7) from the unstandardized order statistics; (2) same as (1) but from the standardized order statistics; (3) the OLS estimator of the regression equation (9) from the unstandardized order statistics; (4) same as (3) but using the standardized sequence of order statistics.

The Monte Carlo experiment consists of the following steps. To gauge the performance of the estimators as a function of the magnitude of the tail decay, we consider the family of symmetric Student-t distributions with degrees of freedom $\theta = \{2, 5, 10, 20\}$ as data generating process (DGP). Note that for Student-t distributions the tail parameter ξ is

equal to the degrees of freedom of the distribution. The DGP is completed by the simulation of two different types of processes given by location parameters $\mu = \{1, 10\}$. These processes are simulated for a sample size $n = 1000$ and for a very large sample size given by $n = 10,000$. By doing so, we aim to capture the differences between the unstandardized and standardized versions of the estimators in large samples. Both estimators require the tuning of the nuisance parameter k. Following the related literature on tail parameter estimation, we compute a battery of estimators of ξ given by values of k in the range $[10, 100]$.

This procedure is repeated for $M = 500$ independent draws of n observations to compute the root mean square error associated to each estimator as $RMSE(\xi) = \sqrt{\sum_{m=1}^{M} (\widehat{\xi} - \xi)^2 / M}$. Figure 1 reports the RMSE of the estimators for $\mu = 1$ and Figure 2 the RMSE for $\mu = 10$. Left panels of both figures report the RMSE for $n = 1000$ and right panels for $n = 10,000$. The dotted lines correspond to the standardized estimators and the solid lines to the unstandardized ones. The thick lines correspond to the Hill estimators and the thin lines to the regression-based estimators. The comparison of the results across figures shows the importance of standardizing the order statistics before estimating the tail decay. The RMSE is significantly smaller for the standardized estimators than for the unstandardized versions independently of the sample size. In fact, the differences remain in Figure 2 even for $n = 10,000$.

The comparison of the results across columns in the same figure provides partial support to the consistency of both types of estimators of ξ. The RMSE slightly decreases as a function of the sample size. Note, however, that the estimators are constructed from a fixed number of order statistics given by k, with k in the range $[10, 100]$. This range is fixed for both $n = 1000$ and $n = 10,000$. The improvement in tail estimation is because the order statistics used for the estimation of ξ are more extreme as the sample size increases. This empirical observation reflects the condition $k \to \infty$ as $k/n \to 0$.

The comparison of the results across panels in the same column shows a decrease in RMSE as the sample size increases. Importantly, there are important differences in the performance of all estimators across values of the parameter ξ. The RMSE increases as a function of ξ confirming the suitability of these estimators for heavy tailed distributions ($\xi > 0$), however, for distributions with exponential decay ($\xi > 20$) the performs is significantly weaker. These findings hold for both values of μ and the tail parameter ξ.

The comparison of the results for single panels allows us to compare the performance between the Hill estimator and the regression-based estimator. The results show some heterogeneity across panels but the overall conclusion is that Hill type estimators perform

better than regression based methods for small values of the location parameter. The opposite result is found for large values of μ. Nervertheless, the standardized Hill estimator tends to perform best for both DGPs.

Similar results are found for the analysis of the left tail and negative values of the location parameter and are omitted for space considerations.

5 Geographical heterogeneity in extreme warming

The recent literature modeling the dynamics of temperatures has found strong empirical evidence of heterogeneity in the evolution of temperatures over time and across regions, see GG2020 and GG2024. The presence of heterogeneity is usually interpreted as evidence of positive trends in distributional characteristics of the distribution of temperatures such as the mean, median, and the quantile process, that is usually accompanied by a negative trend in dispersion measures. The aim of this section is to complement and extend these studies by analyzing the dynamics of extreme temperatures over time. To do this, we apply the trend tests introduced in Definitions 3 and 4 for the tail parameter ξ. The above tests are applied to a panel of monthly temperatures for different regions of the world.

5.1 Data

Our dataset is obtained from the Climatic Research Unit (CRU) at University of East Anglia. The CRU offers monthly and yearly data of land and sea temperatures in both hemispheres from 1850 to the present, collected from different stations around the world. HadCRUT5 is a global temperature dataset, providing gridded temperature anomalies across the world, as well as averages for the hemispheres and for the globe as a whole. CRUTEM5 and HadSST4 are the land and ocean components of this overall dataset, respectively. This database (in particular, the annual temperature of the Northern Hemisphere) has become one of the most widely used to illustrate GW from records of thermometer readings. These records form the blade of the well known "hockey stick" graph, frequently used by academics and other institutions, such as, the IPCC. Our study period begins in 1960 and ends in 2022. This period is the subject of the majority of climatological studies due to the intensity with which the phenomenon of climate change is beginning to manifest itself.

To guarantee the stability of the characteristics over the whole sample, we select only those month-stations units with data for all years in the sample period, which forces us to reduce the sample size. We have also removed stations that present problems of inhome-

geneities (Jones et al., 2012). Applying this procedure to the sample period 1960-2022, we have n=126,900 month-stations units belonging to 11,797 stations. These characteristics are constructed for each year using monthly temperature records. In addition to the globe analysis, we adopt regional and geographical perspectives to make more accurate predictions at the regional level. To do so, we carry out two separate analyses. First, we divide the globe into eight geographical areas: the Arctic Polar Circle, Europe, North America, South America, Asia, Africa, Australia and Antarctic. Applying the strategy described in the previous paragraph, the unit month-station number for the globe is 126,900, 4,332 for the Arctic obtained from 478 stations, 34,368 for Europe obtained from 3,537 stations, 27,348 for North America obtained from 2,447 stations, 10,164 for South America obtained from 478 stations, 38,904 for Asia obtained from 4,939 stations, 12,180 for Africa obtained from 288 stations, 5,424 for Australia obtained from 467 stations and, finally, 588 for the Antarctic obtained from 77 stations. Rather than using an exact political classification the stations are selected according to a rectangle formed by the latitude and longitude that circumscribes each continent. In this way, the latitude variable is given priority over other classifications that strictly consider the political variable. Figure 3 shows the distribution of the selected stations according to the unit month-station criterion for the whole globe for the period 1960-2022, and Figure 4 the different geographical areas into which we have divided the globe.

5.2 Distribution of annual temperatures

This section reports the tail behavior of the distribution of annual temperatures for eight regions recorded over the period 1960 to 2022. These regions are the Antarctic, the Arctic region, Africa, Asia, Australia, Europe, North America and South America. Figure 5 reports the dynamics of average temperatures for each region. There is a positive trend in most of them that suggests that the average annual temperature is warming over time.To obtain further insights into the distribution of annual temperatures we report in Figures 6 and 7 nonparametric kernel estimates of the density function for each region. Each panel includes 63 density functions, with each of them corresponding to a different year of the sample and being obtained as the cross-sectional density function estimated from observations recorded at different weather stations in a given region over a given year. The plots reflect very different patterns across regions.

The distributions of annual temperatures for Asia (b), North America (c), South America (d) and the Arctic region (g) are left skewed. The interpretation of these results is,

however, very different across these regions. For the Arctic region, Asia and North America, the left skeweness is an indication of the presence of extreme negative temperatures. For Asia and North America, these events reflect the heterogeneity of these territories that include areas near the Arctic region and can reach temperatures around -40^o celsius. For the Arctic, these temperatures can reach values close to -60^o celsius. The source for the left skewness for South America is different. The support of the distribution of temperatures in this region is in the range $[0, 40]$ and the mode takes values close to 30^o celsius but there are temperatures that are well below this value. Temperatures on the left tail of the distribution are obtained from weather stations in the Southern Cone of the continent whereas temperatures on the right tail are obtained from weather stations near the Equator. The nonparametric kernel density functions for Europe (a) and Australia (f) are symmetric, however, the support of these distributions is quite different and reflect different features of the distribution and dynamics of annual temperatures that will be discussed below. The density functions for Africa (e) and the Antarctic region (h) are different from the rest. The distribution of Africa is right-skewed with a mode around 15^o celsius and the right tail reaches values near 40^o celsius. The left tail of the distribution is bounded by temperatures near zero degrees celsius. The kernel density function for the Antarctic region is bimodal and reflects the strong heterogeneity in temperatures across weather stations. The Western region is colder than the Eastern region.

5.3 Analysis of trends in extreme temperatures

In the following exercise we study the tail behavior of the distribution of annual temperatures. Table 1 reports a battery of summary statistics for the time series of estimates of the tail parameter ξ obtained from the distribution of temperatures standardized by the cross-sectional sample mean and standard deviation at each point in time. Each tail is considered separately; to add robustness to our findings, the estimates of the tail parameter are computed using different versions of Hill estimator. Methods 1, 2 and 3 correspond to the Huisman et al (2001) correction of three well known estimators of the tail index: Method 1 is the small-sample correction of the Hill estimator; Method 2 is the correction of the generalized least square estimator proposed in Aban and Meerschaert (2004), and Method 3 is the correction of the least squares estimator obtained in Tripathi (2014). Estimates of the tail index are obtained for each region and year of the evaluation period to obtain a sample of 63 time series estimates for each region. The results in Table 1 confirm the reliability of the tail parameter estimates as the results are very similar across estimation

methods. The sample standard deviations are, in general, small providing further support to the average of the tail parameter estimates as informative measures of tail behavior in both tails. The minimum and maximum statistics provide additional information on the time series dispersion of the parameter estimates of ξ.

The following discussion is based on the sample average of the tail parameter estimates reported in the left panel of Table 1, the trend tests in Table 2, and the plots reported in Figure 8 with the evolution of the tail parameters over the evaluation period (1960-2022). The results reveal important heterogeneity across tails and geographical regions. The first region is the Globe that pools together the observations from all regions. The results for this case show important differences across tails. The left tail exhibits a polynomial decay given by values of ξ around 7.5 whereas the right tail exhibits a faster tail decay given by estimates around 17. The trend test is not statistically significant for the left tail but is highly significant (at 1% significance level) providing statistical evidence of a negative trend in the sequence of tail parameter estimates $\widehat{\xi}_t^R$. The interpretation of this test is that the tail parameter decreases over time entailing a fatter tail and, hence, an increased likelihood of positive extreme events. This tail behavior is categorized in Definition 2 as extreme warming of type WE2. The dynamics of the tail parameters for the Globe are not reported for space considerations.

The tail behavior for the distribution of annual temperatures for North America, Asia and the Antarctic region shows similar patterns in both tails but the magnitude of the slope coefficient for North America and Asia is twice as large as for the Globe. The three regions exhibit extreme warming of type WE2. The negative trend in the tail parameter estimates is clearly visible in panels (b) and (c) of Figure 8 and panel (h) of Figure 9. For North America, the estimate of the tail parameter in 1960 is close to exponential with a value near 20. The time series has steadily decreased over the last sixty years and the estimate of the tail parameter ξ for 2022 is around 16. The behavior of the right tail parameter for Asia is similar although the magnitude of the trend parameter is slightly stronger and there are also some interesting nonlinearities during the period 1970-1990. The case of the Antarctic region reveals stronger polynomial decay in both tails than for the other two regions but there is still clear evidence of a negative trend with values of the tail parameter close to 5 in the last years of the sample.

The case of Europe reveals an average fatter tail in both regions than for Asia and North America. However, the trend test in table 2 does not uncover a trend in any of the tails. Similarly, the dynamics of the time series of parameter estimates reported in panel (a) of

figure 8 are stable over the evaluation period. These patterns are compatible with the type WE0 that corresponds to the absence of extreme warming in the tails. This does not imply that there is warming in other distributional characteristics such as the mean (see figure 5) and findings in GG2020 and GG2024. Similar results for the trend tests are found for Africa. There is no statistical evidence of a time trend in either tail of the distribution of annual temperatures. However, in contrast to Europe, the average tail estimates reveal fatter tails for Africa than for Europe indicating a higher probability of extreme temperatures for this region. This is confirmed by the evolution of the tail parameter estimates reported in panel (e) of figure 9. Similar pattern in the tails is observed for the Polar region. The tail behavior in the left tail exhibits fatter tails than for the right tail indicating a greater probability of extreme events in the left tail, however, there is no evidence of a time trend in the evolution of temperatures for this region. These patterns are consistent with the type of warming WE0.

The results for South America and Australia point in a different direction. The warming process in the extremes is different. The sign of the slope coefficient of the regression equation (5) is positive for both tails and statistically significant in all cases except the left tail of South America. These results provide evidence of a thinner left tail over time for both regions. This behavior of the extreme temperatures in the left tail is classified as type WE1 in definition 2 and corresponds to an increase in the negative extreme temperatures resulting in milder temperatures in the left tail of the distribution. The average value of the tail parameter estimates is, nevertheless, lower than for the regions in the North hemisphere being around 5 and 8 for South America and Australia, respectively. The results for the right tail are similar quantitatively indicating a positive trend that is clearly visible from panels (d) and (f) in figure 9. The interpretation is, however, completely different. The positive trend in the right tail indicates a lower probability of extreme positive temperatures over time. The results from both tails combined provide evidence of a decrease in the dispersion of temperatures for these regions over time. Temperatures shift to the right of the distribution with negative extreme shifting faster and positive extremes shifting slower than the rest of quantiles.

The above results show clear heterogeneity in the warming process of extreme temperatures. Importantly, our empirical findings suggest evidence of four different patterns in the behavior of extreme temperatures that seem related to the geographical location of the regions under investigation. The only exception is the Antarctic region that shares similarities in tail trend behavior with North America and Asia in both tails.

The following exercise aims to test for the presence of cotrending in the dynamics of extreme temperatures for regions sharing the same patterns. We focus on the pairs North America and Asia; Europe and Africa, and South America and Australia. To do this, we implement the test in Definition 4 for the presence of cotrending between the tail parameters of different pairs of regions. The purpose of the analysis is to assess statistically if the warming process in the extremes is at the same pace across regions. We focus on pairs of regions that already show evidence of warming in the extremes of a specific type (WE1 or WE2) and that show similar patterns. In particular, we test for cotrending between the right tail parameters of Asia and North America, and the left and right tail parameters of South America and Australia. We complete the analysis with the comparison of tail dynamics between the Arctic region and Europe in the left tail. Although the estimates of ξ are not statistically significant for any of these regions the magnitude of the slope parameters in Table 2 is roughly similar. In this scenario it may be of interest to test if the trends in the tail parameters for these regions are similar providing further support to the hypothesis that the minimum temperatures for Europe and the Arctic region are warming up at the same pace than the remaining quantiles of the distribution of annual temperatures.

The results of the test of cotrending in the tails are presented in Table 3. Our analysis is concerned with modeling long-term dynamics, hence our interest in the analysis of trends. The overall conclusion of the analysis is that there is no statistical evidence to reject the hypothesis of cotrending in the tails between any pair of the above regions. A more detailed analysis reveals that for the pair Asia-North America the slope coefficient γ of the regression model (6) in the right tail is -0.004 and the corresponding p-value is 0.886. Similarly, the comparison of the dynamics of the tail parameters in the left tail for the pair South America-Australia yields a parameter estimate of -0.005 with a p-value of 0.437. For the right tail, the parameter estimate for γ is 0.013 and the corresponding p-value is 0.515. Finally, the comparison of the dynamics in the left tail for the pair Arctic region-Europe reports a value of -0.003 for the slope parameter estimate in the left tail, with a p-value of 0.910, and $-0.014\,[0.590]$ for the right tail.

The above results show clear evidence of cotrending in the tails, however, we also find significant statistical evidence to reject the equality of the tail parameters for all pairs and in both tails. This is captured through the intercept of the regression equation (6) and also shown by the difference in magnitude of the tail parameters across regions observed in Figures 8 and 9.

6 Conclusion

Understanding the heterogeneity in worldwide temperatures is important for predicting future dynamics in climate change and guide policy. In this paper, we have analyzed the dynamics of extreme temperatures using the methodology proposed in GG2020 to detect the presence of time trends in the distributional characteristics of annual temperatures. This paper complements previous studies by focusing on the dynamics of the tail parameter for both tails. For a very general class of distributions, this parameter completely drives the tail decay.

As a byproduct of our study, we have also analyzed the finite-sample performance of popular estimators of the tail parameter such as the Hill estimator and regression-based estimators. Taking advantage of a thorough simulation study, we conclude that the versions of these estimators constructed from standardized order statistics outperform the typical estimators constructed from unstandardized sequences.

Using a panel of observations on monthly temperatures from a large cross section of weather stations, we have estimated the tail parameters from cross-sectional distributions applied to each region and obtained a time series of tail parameter estimates over the period 1960 to 2022. Our empirical results show clear heterogeneity in the warming process of extreme temperatures. There are four different patterns that seem related to the geographical location of the regions under investigation. Thus, North America, Asia and the Antarctic regions are affected by a warming process of type WE2. Europe, Africa and the Arctic region do not exhibit warming in the extremes despite a steady increase in their quantiles (see GG2020) suggesting that the behavior of the distribution of temperatures is compatible with a type WE0. In the South hemisphere, South America and Australia show a pattern that is compatible with type WE1 and suggests warming of extreme temperatures in the left tail. Both regions also show a drop in dispersion in the extreme temperatures in the right tail which suggests that the distribution of annual temperatures is becoming more concentrated around the mode.

References

[1] Aban, I.B., and M.M. Meerschaert (2001). Shifted Hill's estimator for heavy tails. *Communications in Statistics. Simulation Comput.* 30, 949–962.

[2] Aban, I.B., and M.M. Meerschaert (2004). Generalized least-squares estimators for the thickness of heavy tails. *Journal of Statistical Planning and Inference* 119, 341-352.

[3] Adams, R. M., C. Rosenzweig, R. M. Peart, J. Ritchie, J. To, B. A. McCarl, J.D. Glyer, R.B. Curry, J.W. Jones, K.J. Boote, and L.H. Jr. Allen (1990). Global Climate Change and US Agriculture. Nature 345, 219-224.

[4] Beirlant, J., P. Vynckier, and J.L. Teugels (1996). Tail estimation, Pareto quantile plots, and regression diagnostics. *Journal of the American Statistical Association* 91, 1659–1667.

[5] Danielsson, J., D.W. Jansen, and C.G. De vries (1996). The method of moments ratio estimator for the tail shape parameter. *Communications in Statistics - Theory and Methods* 25 (4), 711-720.

[6] de Haan, L. (1976). Sample extremes: an elementary introduction. *Statistica Neerlandica* 30 (4), 161-172.

[7] Dekkers, A.L.M., J.H.J. Einmahl, and L. de Haan (1989). A Moment estimator for the index of an extreme-value distribution. *The Annals of Statistics* 17 (4), 1833-1855.

[8] Drees (1995). Refined Pickands estimators of the extreme value index. *The Annals of Statistics* 23 (6), 2059-2080.

[9] Embrechts, P., C. Klüppelberg, and T. Mikosch (1997). Modelling Extremal Events for Insurance and Finance. New York: Springer.

[10] Fedotenkov, I. (2018). A review of more than one hundred Pareto-tail index estimators. Munich Personal RePEc Archive. Paper No. 90072. Available at `https://mpra.ub.uni-muenchen.de/90072/`

[11] Gabaix, X. (1999). Zipf's Law for Cities: An Explanation. *Quarterly Journal of Economics* 114, 739-767.

[12] Gabaix, X., and Y. Ioannides (2004). The Evolution of City Size Distributions. In *Handbook of Regional and Urban Economics* Vol. 4, eds. V. Henderson and J.-F. Thisse, Amsterdam: Elsevier North-Holland, 2341-2378.

[13] Gabaix, X., and R. Ibragimov (2012). Rank -1/2: A Simple Way to Improve the OLS Estimation of Tail Exponents. *Journal of Business and Economic Statistics* 29 (1), 24-39.

[14] Gadea-Rivas, M.D., and J. Gonzalo (2020). Trends in distributional characteristics: Existence of global warming. *Journal of Econometrics* 214, 153-174.

[15] Gadea-Rivas, M.D., and J. Gonzalo (2024). Climate change heterogeneity: A new quantitative approach. Working Paper Universidad Carlos III de Madrid.

[16] Gnedenko, B.V. (1943). Sur la distribution limite du terme maximum d'une serie aleatoire. *Annals of Mathematics* 44 (3), 423-453.

[17] Hansen, J. and S. Lebedeff (1987). Global Trends of Measured Surface Air Temperature. *Journal of Geophysics* 92, 13345-13372.

[18] Hansen, J. and S. Lebedeff (1988). Global Surface Air Temperature: Update through 1987. *Geophysical Res. Letters* 15, 323-326.

[19] Hill, B. (1975). A simple general approach to inference about the tail of a distribution. *Annals of Statistics* 3, 1163–1173.

[20] Jones P.D., D.H. Lister, T.J. Osborn, C. Harpham, M. Salmon, and C.P. Morice (2012). Hemispheric and large-scale land surface air temperature variations: an extensive revision and an update to 2010. *Journal of Geophysical Research* 117, 1-29.

[21] Huisman, R., K.G. Koedijk, C.J.M. Kool, and F. Palm (2001). Tail-Index Estimates in Small Samples. *Journal of Business and Economic Statistics* 19 (2), 208-216.

[22] Katz and Brown (1992). Extreme events in a changing climate: variability is more important than averages. *Climatic Change* 21, 289-302.

[23] Kratz, M., and S. Resnick (1996). The qq-estimator and heavy tails. *Communications in Statistics. Stochastic Models* 12, 699–724.

[24] Mearns, L.O., R.W. Katz, and S.H. Schneider (1984). Extreme High-Temperature Events: Changes in their Probabilities with Changes in Mean Temperature. *Journal of Clim. Appl. Meteorol.* 23, 1601-1613.

[25] Mitchell, J. E B., S. Manabe, V. Meleshko, and T. Tokioka (1990). Equilibrium Climate Change - and its Implications for the Future. In J. T. Houghton, G. J. Jenkins, and J. J. Ephranms (eds.), Climate Change: The IPCC Scientific Assessment. Cambridge University Press, Cambridge, pp. 131 - 172.

[26] Nicolau, J. and P.M. Rodrigues (2019). A New Regression-Based Tail Index Estimator. *The Review of Economics and Statistics* 101 (4), 667-680.

[27] Pickands III, J. (1975). Statistical Inference Using Extreme Order Statistics. *The Annals of Statistics* 3, 119-131.

[28] Rosen, K. T., and M. Resnick (1980). The Size Distribution of Cities: An Examination of the Pareto Law and Primacy. *Journal of Urban Economics* 8, 165-186.

[29] Tripathi, Y. M., S. Kumar, and C. Petropoulos (2014). Improved estimators for parameters of a Pareto distribution with a restricted scale. *Statistical Methodology* 18, 1–13.

[30] von Mises, R. (1936). La distribution de la plus grande de n valeurs. Rev. Math. Union Interbalcanique 1, 141-160.

[31] Wigley, T. M. L.. (1985). Impact of Extreme Events. Nature 316, 106-107.

[32] Wigley, T. M. L. (1988). The Effect of Changing Climate on the Frequency of Absolute Extreme Events. Climate Monitor 17, 44-55.

Table 1: Summary statistics of the sequence of tail parameter estimators using Huisman et al (2001) type estimator.

	Sample mean						Standard deviation						Minimum						Maximum					
	Left			Right			Left			Right			Left			Right			Left			Right		
Region/Method	1	2	3	1	2	3	1	2	3	1	2	3	1	2	3	1	2	3	1	2	3	1	2	3
Globe	8.1	7.8	7.0	18.0	17.1	15.5	1.3	1.2	1.2	2.2	2.1	2.0	6.3	6.0	5.4	14.2	13.5	12.0	11.7	11.3	10.3	24.2	23.1	20.9
Europe	11.3	10.8	9.8	17.1	16.4	14.9	3.5	3.4	3.1	2.5	2.4	2.2	5.1	4.8	4.3	9.8	9.3	8.4	21.7	20.8	18.8	23.5	22.5	20.5
Asia	16.8	16.1	14.6	18.2	17.3	15.7	3.1	3.0	2.7	2.7	2.6	2.4	10.9	10.4	9.4	13.4	12.8	11.4	24.8	23.7	21.5	25.3	24.2	21.9
North America	12.2	11.6	10.6	19.8	18.9	17.2	1.7	1.6	1.5	3.9	3.8	3.5	9.1	8.7	7.9	13.5	12.9	11.6	16.7	16.0	14.6	34.7	33.3	30.6
South America	6.6	6.3	5.7	14.6	13.9	12.6	0.6	0.6	0.6	2.9	2.8	2.5	5.3	5.1	4.6	9.4	8.9	8.1	8.5	8.1	7.4	22.3	21.3	19.3
Africa	5.3	4.9	4.2	5.2	4.9	4.2	0.7	0.6	0.6	0.8	0.7	0.7	4.1	3.8	3.3	3.9	3.6	3.1	7.5	7.0	6.1	9.3	8.7	7.6
Australia	8.6	8.3	7.5	9.1	8.7	7.9	0.8	0.8	0.7	1.1	1.1	1.0	7.0	6.7	6.1	6.7	6.4	5.8	11.5	10.9	9.8	12.8	12.2	11.1
Arctic region	8.3	7.9	7.2	14.1	13.5	12.2	1.3	1.2	1.1	2.6	2.4	2.2	5.8	5.5	5.0	9.3	8.9	8.1	11.5	11.0	10.1	22.3	21.3	19.2
Antarctic region	1.7	1.5	1.0	9.6	8.4	6.0	0.6	0.5	0.4	3.3	3.0	2.5	0.5	0.4	0.2	4.2	3.4	1.8	3.2	2.9	2.2	22.4	20.1	15.3

Note: These summary statistics are computed from a time series of tail parameter estimates of ξ obtained from the small-sample correction estimator developed in Huisman et al (2001) applied to different versions of Hill estimator. Method 1 is the Huisman et al estimator constructed from a sequence of Hill estimators with different thresholds. Similarly, Method 2 is based on a sequence of best linear unbiased estimators with different thresholds; and Method 3 is based on a sequence of OLS estimators. The time series of estimates corresponds to annual data from 1960 to 2022.

Table 2: Trending analysis for standardized temperatures under regression equation (5).

	Left tail			Right tail		
Region/Method	1	2	3	1	2	3
Globe	-0.012	-0.011	-0.010	-0.038^{**}	-0.037^{**}	-0.033^{**}
	[0.189]	[0.205]	[0.244]	[0.012]	[0.013]	[0.014]
Europe	-0.010	-0.010	-0.009	0.007	0.007	0.005
	[0.700]	[0.699]	[0.667]	[0.676]	[0.695]	[0.739]
Asia	0.002	0.001	0.002	-0.080^{***}	-0.077^{***}	-0.070^{***}
	[0.953]	[0.981]	[0.957]	[0.000]	[0.000]	[0.000]
North America	0.008	0.008	0.007	-0.076^{***}	-0.073^{***}	-0.068^{***}
	[0.481]	[0.477]	[0.470]	[0.005]	[0.005]	[0.005]
South America	0.006	0.006	0.006	0.034^{*}	0.033^{*}	0.031^{*}
	[0.142]	[0.143]	[0.145]	[0.083]	[0.081]	[0.078]
Africa	0.000	0.001	0.001	-0.007	-0.006	-0.005
	[0.920]	[0.900]	[0.853]	[0.224]	[0.226]	[0.233]
Australia	0.011^{**}	0.011^{**}	0.009^{*}	0.021^{***}	0.021^{***}	0.019^{***}
	[0.040]	[0.044]	[0.054]	[0.005]	[0.005]	[0.005]
Arctic region	-0.013	-0.012	-0.012	-0.007	-0.006	-0.005
	[0.156]	[0.151]	[0.139]	[0.698]	[0.706]	[0.724]
Antarctic region	0.003	0.003	0.002	-0.039^{*}	-0.036^{*}	-0.028^{*}
	[0.391]	[0.396]	[0.411]	[0.089]	[0.089]	[0.093]

Note: P-values are in square brackets. $*$, $**$, $***$ denote statistical significance of the slope parameter estimate β of the LS regression equation (5) at 10%, 5% and 1% significance levels, respectively. The response variable is the sequence of tail parameter estimates $\widehat{\xi}_t^L$ and $\widehat{\xi}_t^R$ obtained under different estimation methods. Method 1 is the Huisman et al estimator constructed from a sequence of Hill estimators with different thresholds. Similarly, Method 2 is based on a sequence of best linear unbiased estimators with different thresholds; and Method 3 is based on a sequence of OLS estimators. The time series of estimates corresponds to annual data from 1960 to 2022.

Table 3: Cotrending analysis for standardized temperatures under regression equation (6).

	Left tail			Right tail		
Region/Method	1	2	3	1	2	3
Asia - North Am.	-0.008	-0.007	-0.005	-0.004	-0.004	-0.003
	[0.714]	[0.738]	[0.794]	[0.886]	[0.892]	[0.904]
South Am. - Aust.	-0.005	-0.003	-0.003	0.013	0.013	0.012
	[0.437]	[0.460]	[0.512]	[0.515]	[0.518]	[0.491]
Arctic - Europe	-0.003	-0.003	-0.002	-0.014	-0.013	-0.011
	[0.910]	[0.910]	[0.917]	[0.590]	[0.607]	[0.647]

Note: P-values are in square brackets. $*$, $**$, $***$ denote statistical significance of the slope parameter estimate γ of the LS regression equation (6) at 10%, 5% and 1% significance levels, respectively. The response variable is the difference of tail parameter estimates $\widehat{\xi}_t^A - \widehat{\xi}_t^B$, with A and B the regions on the first column. Method 1 is the Huisman et al estimator constructed from a sequence of Hill estimators with different thresholds. Similarly, Method 2 is based on a sequence of best linear unbiased estimators with different thresholds; and Method 3 is based on a sequence of OLS estimators. The time series of estimates corresponds to annual data from 1960 to 2022.

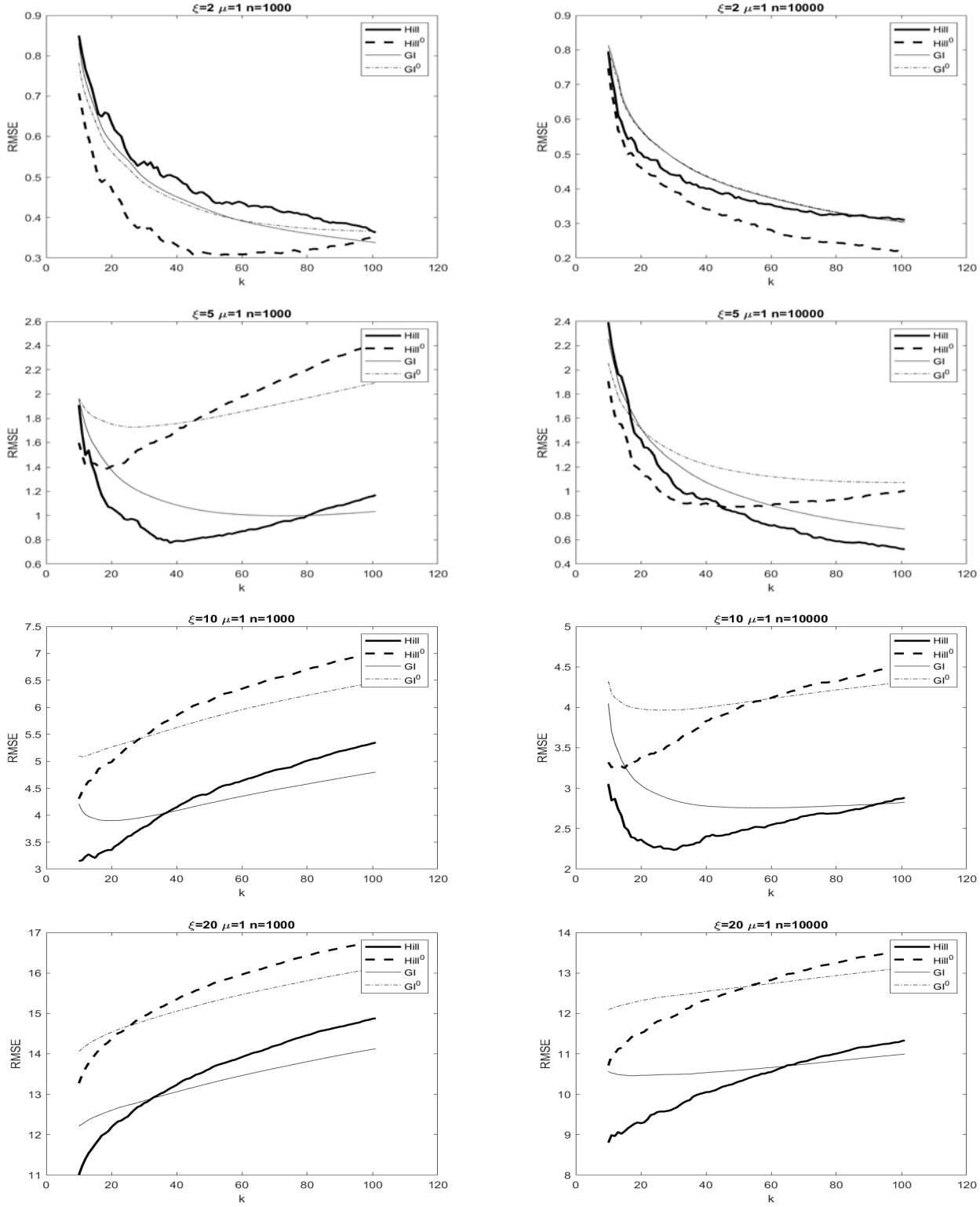

Figure 1: Root mean square error for Hill estimator in (7) and regression-based estimator in (9) for $n = 1,000$ (left panel) and $n = 10,000$ (right panel); k characterizes the threshold sequence $x_{k:n}$ and ranges in the interval $[10, 100]$. The data generating process is a Student-t distribution with ξ degrees of freedom, with $\xi = \{2, 5, 10, 20\}$, and location parameter $\mu = 1$.

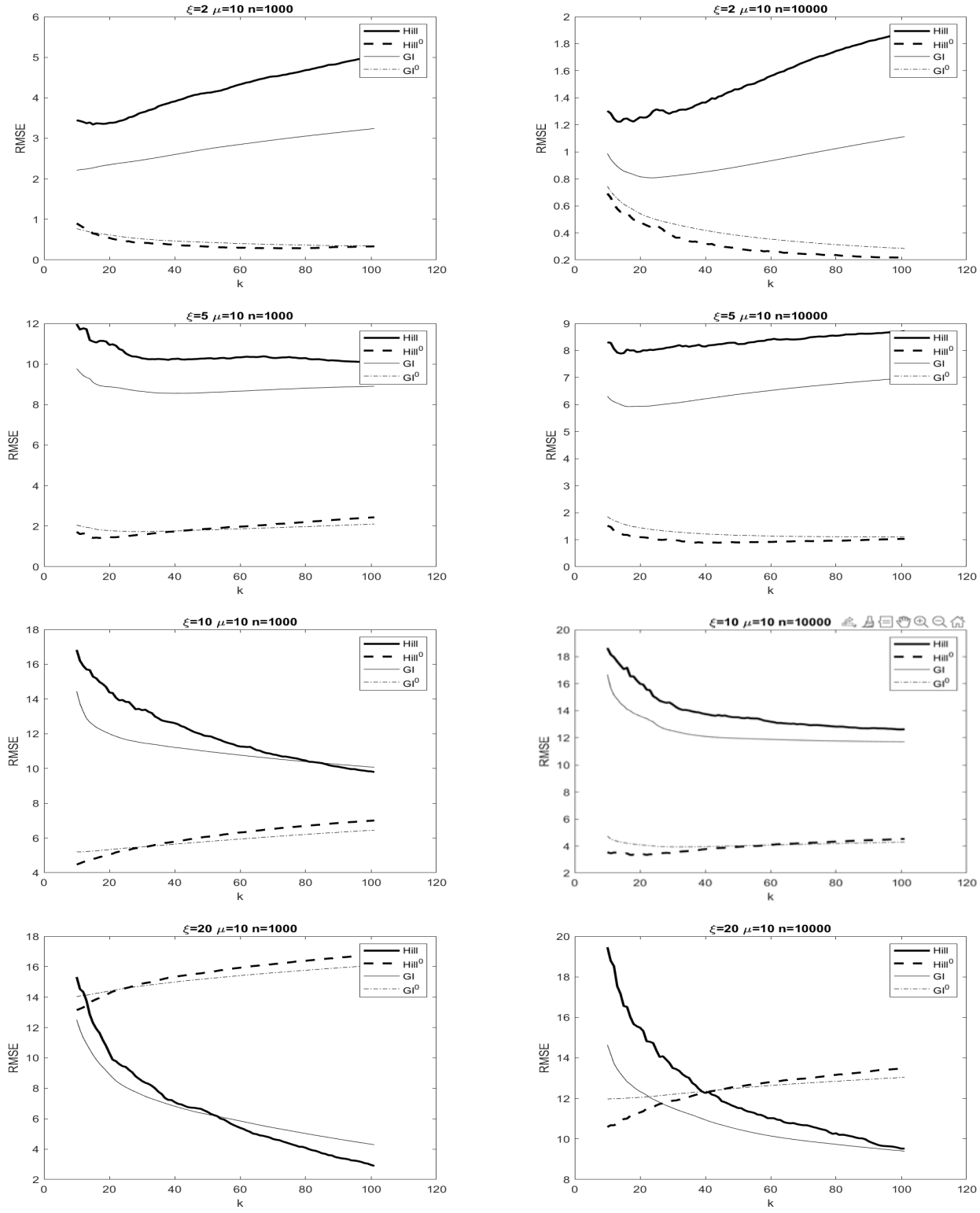

Figure 2: Root mean square error for Hill estimator in (7) and regression-based estimator in (9) for $n = 1,000$ (left panel) and $n = 10,000$ (right panel); k characterizes the threshold sequence $x_{k:n}$ and ranges in the interval $[10, 100]$. The data generating process is a Student-t distribution with ξ degrees of freedom, with $\xi = \{2, 5, 10, 20\}$, and location parameter $\mu = 10$.

Figure 3: Location of weather stations 1960-2022.

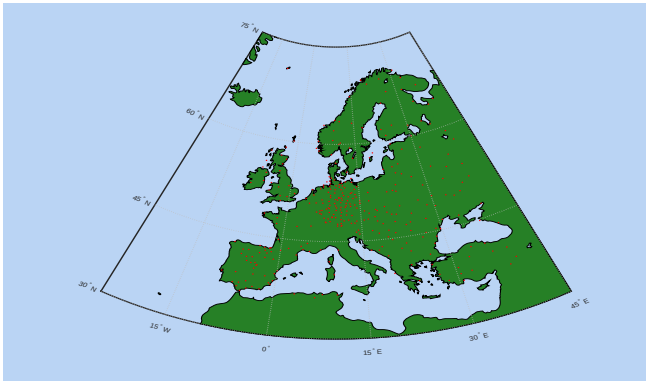

(a) Europe

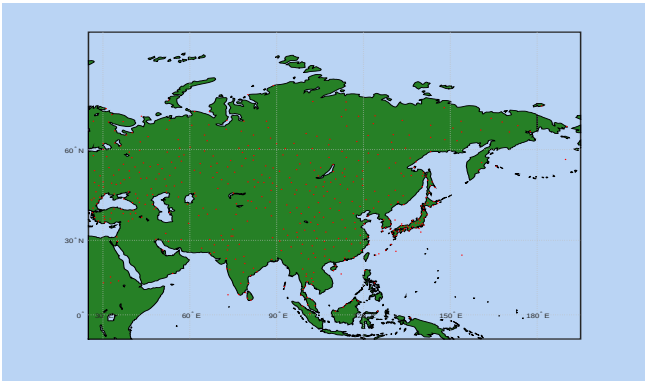

(b) Asia

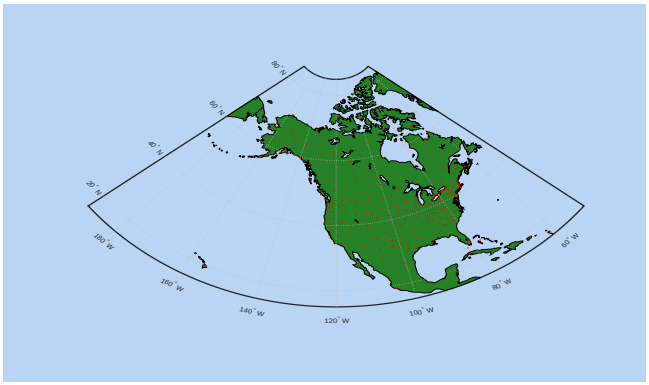

(c) North America

(d) South America

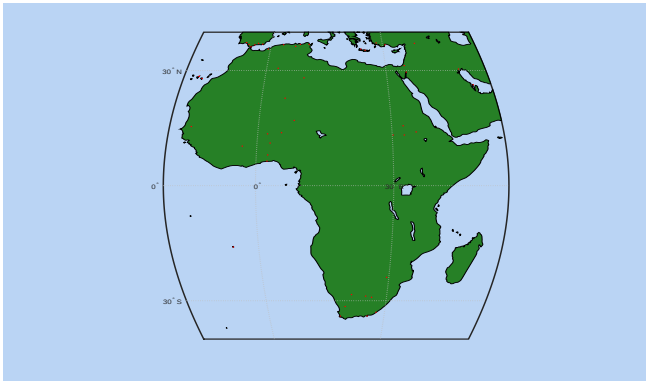

(e) Africa

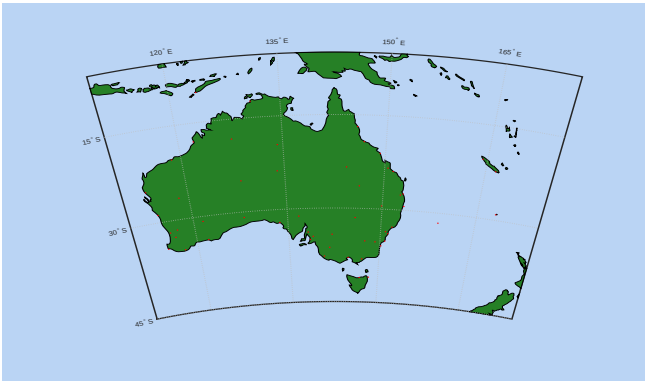

(f) Australia

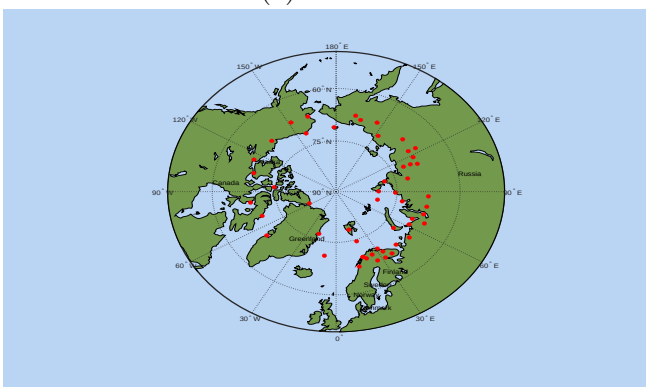

(g) Arctic region

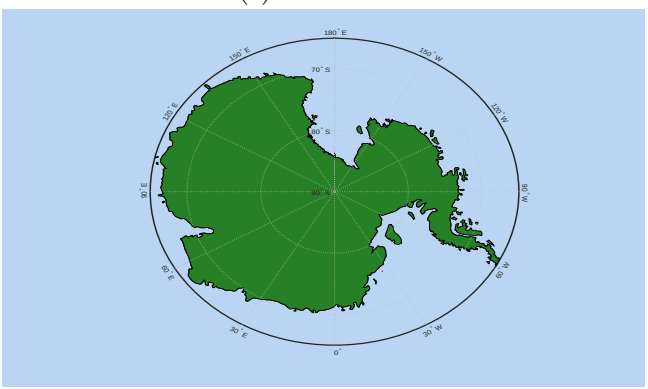

(h) Antarctic region

Figure 4: Division of the globe into geographical regions characterized by continents.

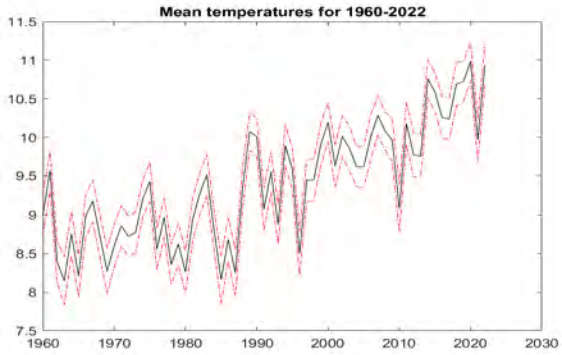

(a) Europe

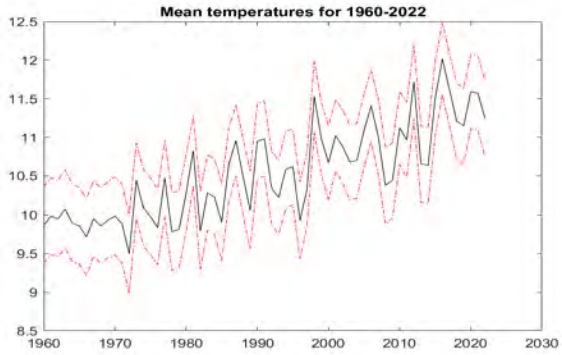

(b) Asia

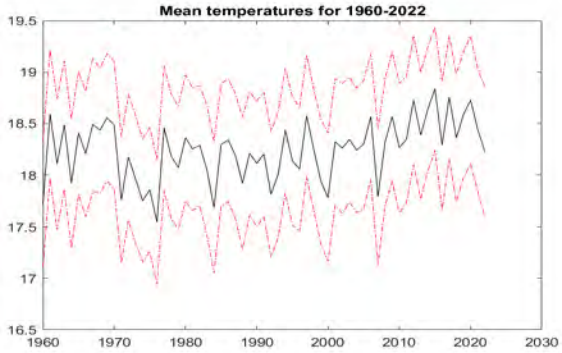

(c) North America

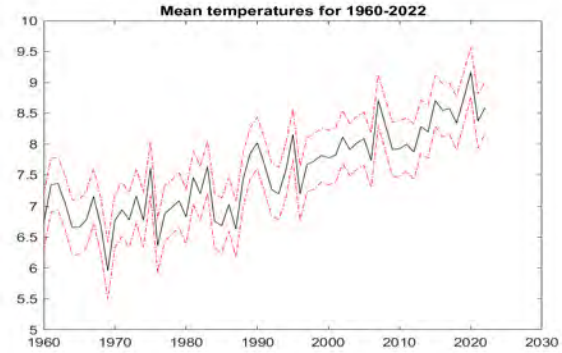

(d) South America

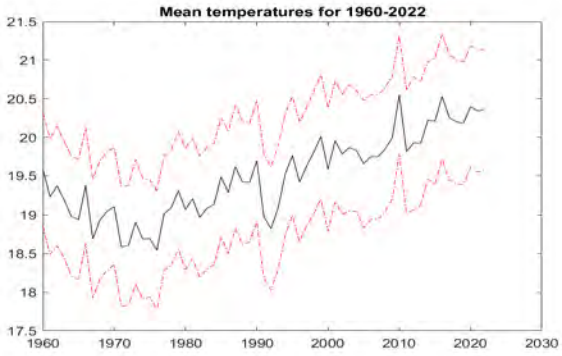

(e) Africa

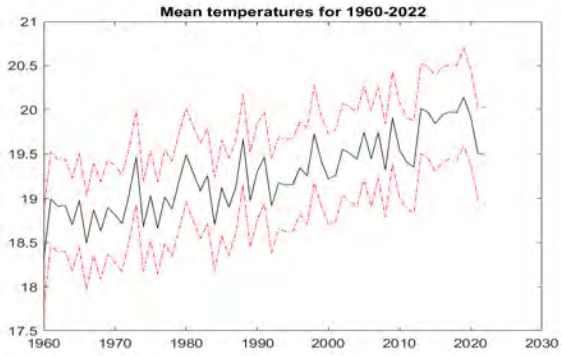

(f) Australia

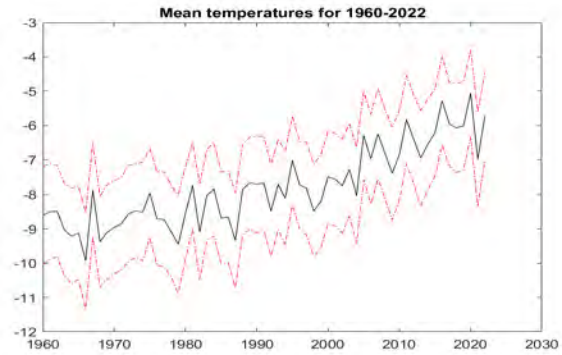

(g) Artic region

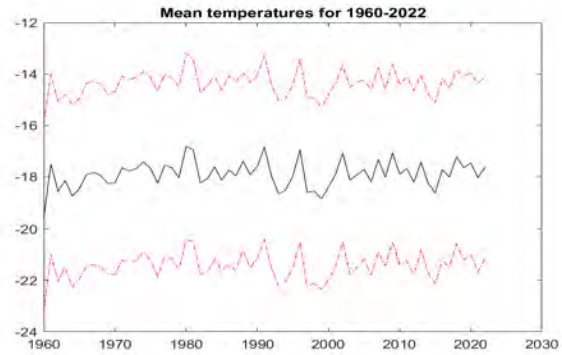

(h) Antartic region

Figure 5: Dynamics of mean temperatures by continents over the period 1960-2022. Dotted lines are 95% confidence intervals.

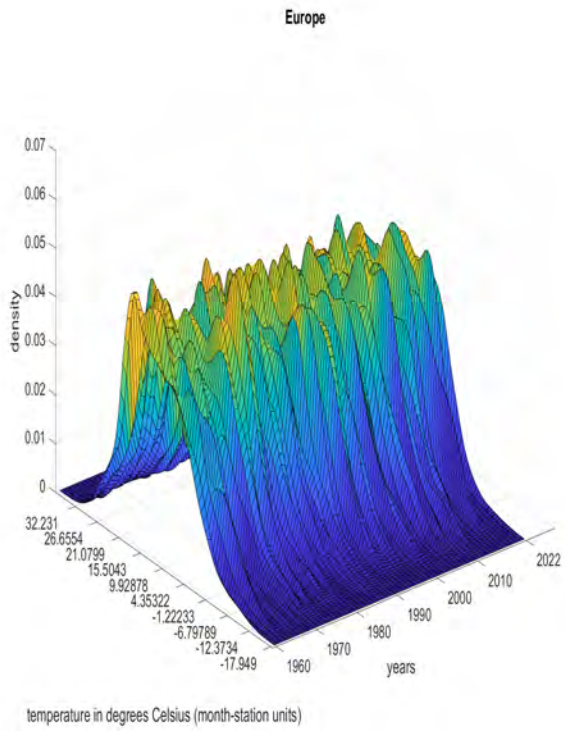

(a) Europe

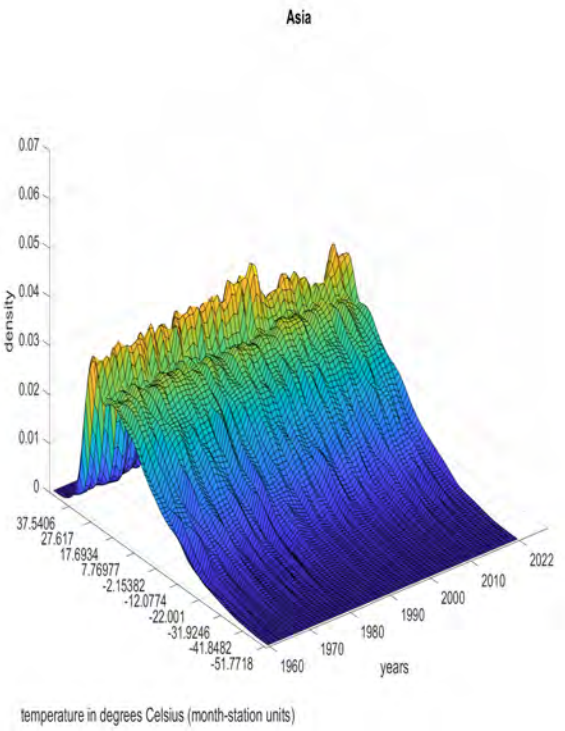

(b) Asia

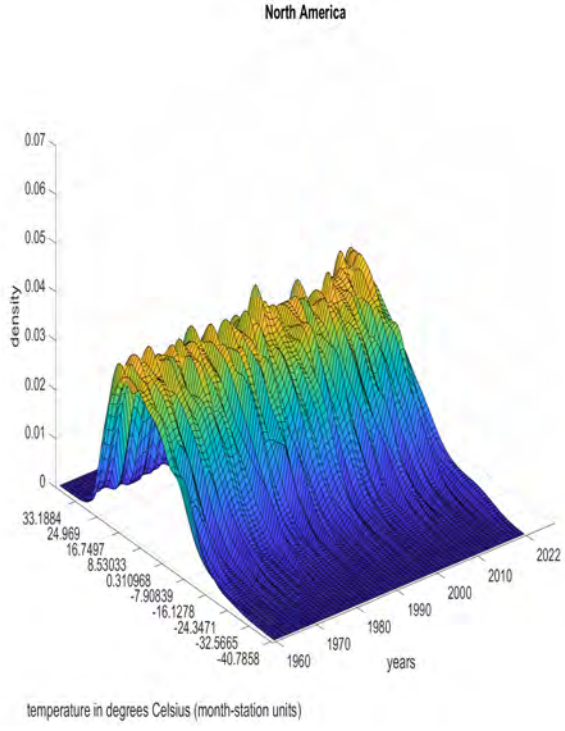

(c) North America

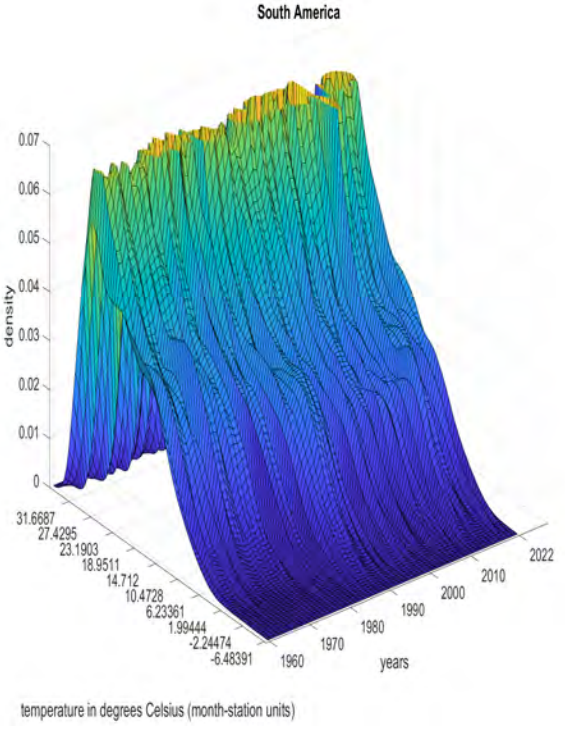

(d) South America

Figure 6: Kernel density function estimates for annual temperatures (1960-2022).

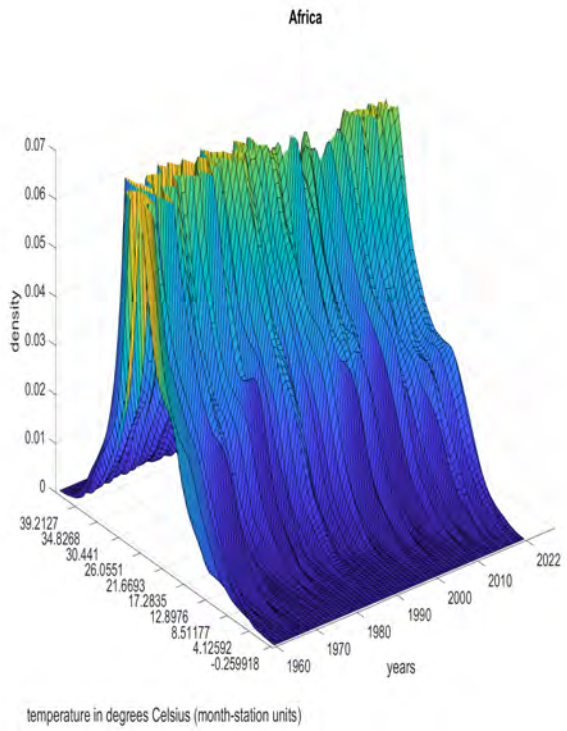

(e) Africa

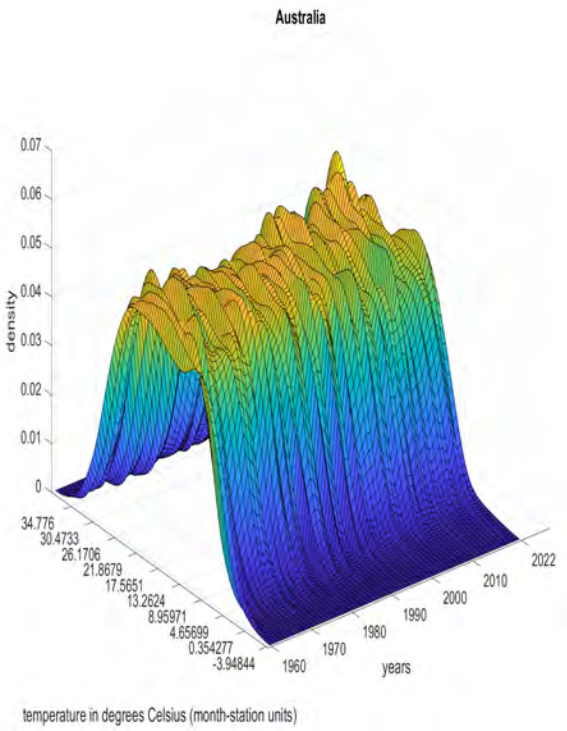

(f) Australia

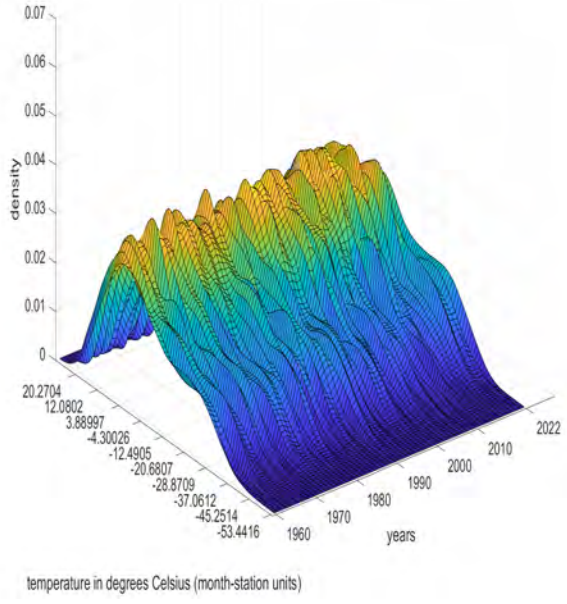

(g) Arctic region

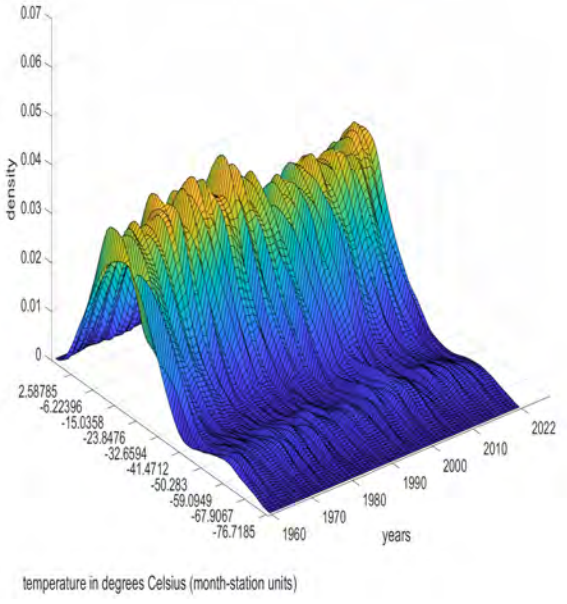

(h) Antarctic region

Figure 7: Kernel density function estimates for annual temperatures (1960-2022).

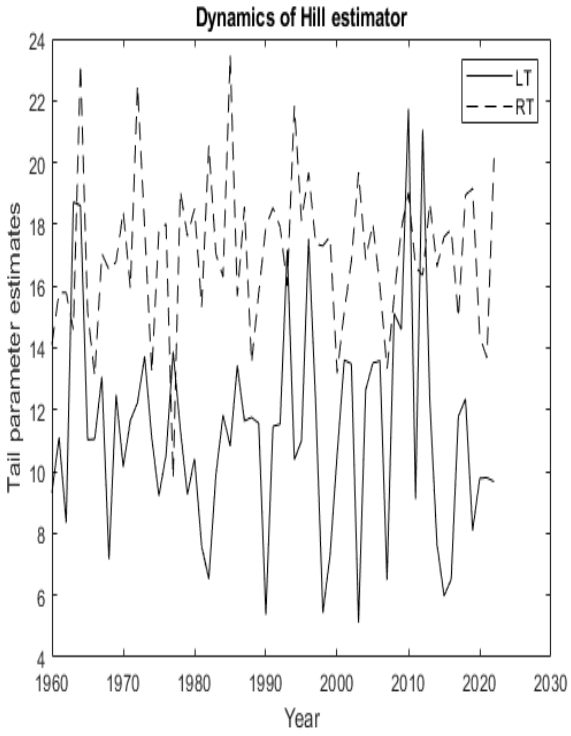

(a) Europe

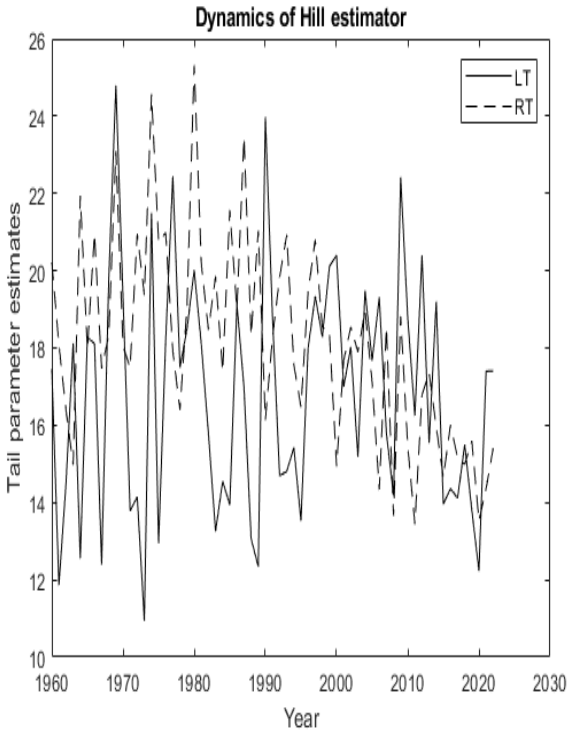

(b) Asia

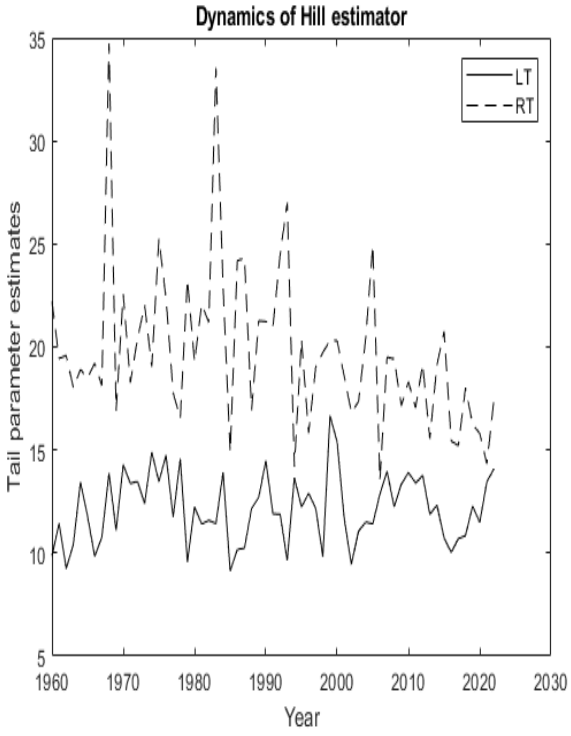

(c) North America

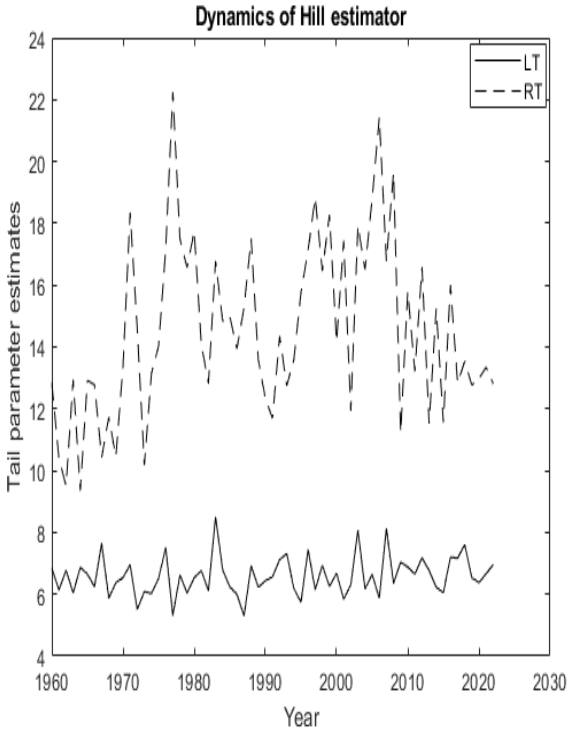

(d) South America

Figure 8: Dynamics of Huisman et al tail index estimator based on Hill estimator for annual temperatures (1960-2022).

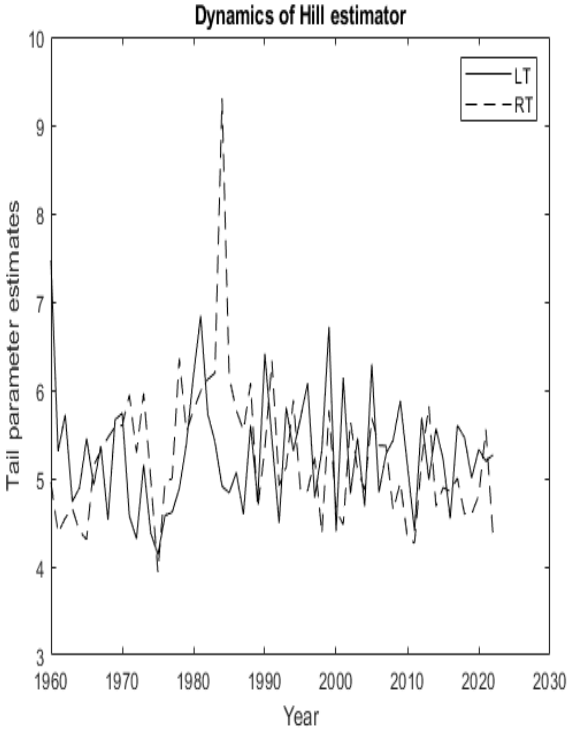

(e) Africa

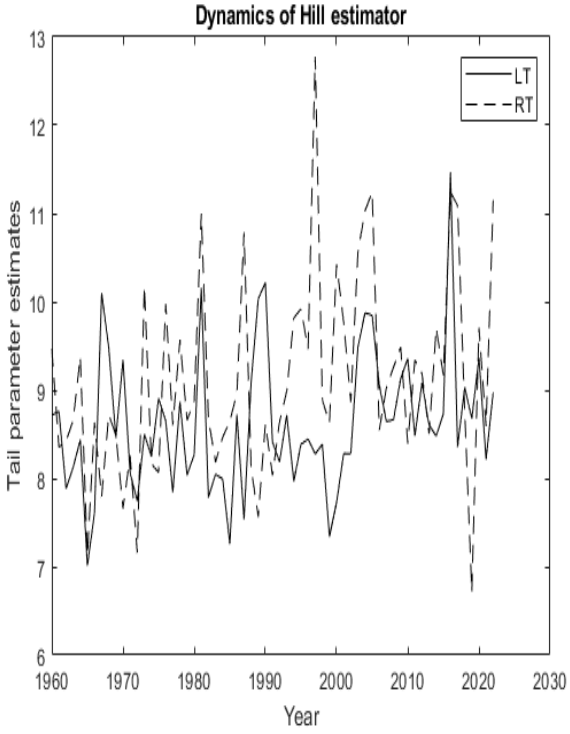

(f) Australia

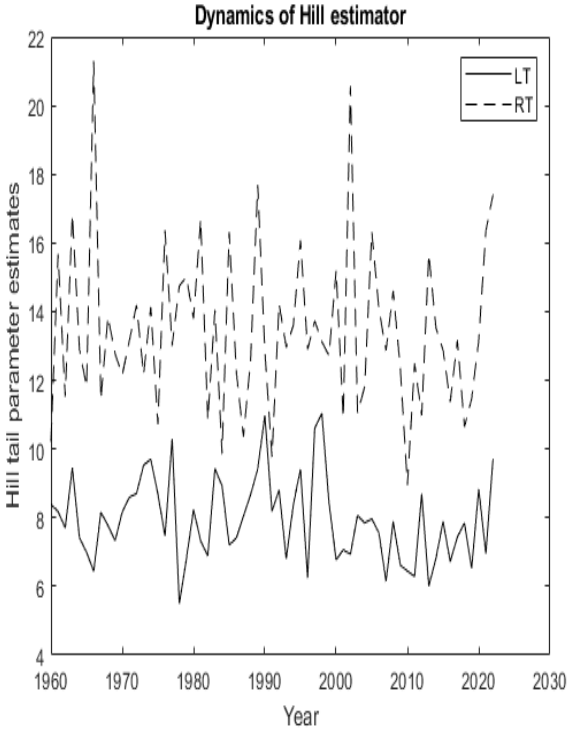

(g) Arctic region

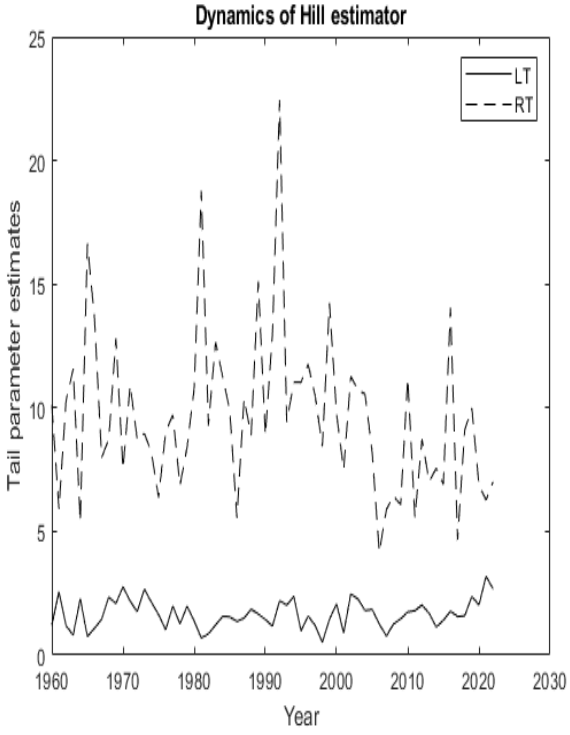

(h) Antarctic region

Figure 9: Dynamics of Huisman et al tail index estimator based on Hill estimator for annual temperatures (1960-2022).